

# AUTOMATIC MODELING OF LASER POINT CLOUDS BY STATISTICAL ANALYSIS OF SURFACE CURVATURE VALUES

Fabio Crosilla, Domenico Visintini, Francesco Sepic

Department of Georesources & Territory, University of Udine, via Cottonificio, 114 I-33100 Udine, Italy  
fabio.crosilla@uniud.it; domenico.visintini@uniud.it; francesco.sepic@e-laser.it

**KEY WORDS:** Laser scanning, Classification, Statistical analysis, Spatial modeling.

## ABSTRACT

Laser scanning measurements are characterized by errors of different kind and simplified analytical models are normally applied to estimate the differential terms used to locally compute the object surface curvature values. The paper synthesizes the statistical analyses of the non parametric model applied, and of the *Gaussian K* and *mean H* local curvatures values, as already proposed by the authors in recent papers. The statistical analyses are based at first on a Chi-Square test applied to verify the second order Taylor's expansion model fulfilment. Afterwards, the variance-covariance propagation law is applied to the estimated differential terms to calculate the covariance matrix of a vector containing the *Gaussian* and the *mean* curvature estimates and an *F* ratio test is applied to verify their significance. By analyzing the test results for *K* and *H*, and their sign, a reliable classification of the whole point cloud into its geometrical basic types is carried out. To perform the units segmentation, by analytically detecting discontinuity lines, an analysis of the extended Taylor's model to the third and fourth order terms is mentioned. Some numerical experiments on real noisy laser data relating to a complex surface of a church apse confirm the validity of the method proposed.

## 1. INTRODUCTION

The paper synthesizes the most recent researches conducted by the authors in the direction of a reliable geometrical classification method of the laser point clouds, whose analytical aspects and whose laser scanning applications have been presented at the XXI ISPRS General Congress (Crosilla, Visintini and Sepic, 2008) and recently accepted for publication on Applied Geomatics (Crosilla, Visintini and Sepic, 2009).

The procedure is fundamentally based on the statistical analysis of the *Gaussian K* and *mean H* curvatures, obtained for a certain surface point by the differential terms of a second order Taylor's expansion. The weighted least squares estimate of the unknown vector, collecting the differential terms, is obtained by considering a selected number of surrounding points, within a bandwidth radius, and by applying a weighting function, depending on their distance from the central point.

Since the measurements noise worsens the data quality and the non parametric modeling simplifies the surface true shape, the curvature values have to be statistically verified, i.e. also the variances of the estimated values have to be taken into account. To verify the fulfilment of the second order Taylor's expansion model, a Chi-Square ratio test is applied to the estimated variance factor and to the a priori measurement variance.

If the null hypothesis is accepted, the corresponding local *Gaussian K* and *mean H* curvature values, as well as the principal curvatures, can be reliably determined by the locally estimated surface differential terms.

A statistical analysis of the curvature vector, containing the *Gaussian* and the *mean* curvature values, is then carried out. By applying the variance-covariance propagation law, the covariance matrix of the curvature vector is obtained. A Fisher ratio test is subsequently applied to verify the significance of the curvature values. If the null hypothesis is accepted, the surface can be locally accepted as planar. If the null hypothesis is rejected a ratio test for each *K* and *H* curvatures is carried out. By simultaneously analyzing the sign and the values of *K* and *H*, a classification of the points is achievable according to the following surfaces basic types: hyperbolic (if  $K < 0$ ), parabolic ( $K = 0$  but  $H \neq 0$ ), planar ( $K = H = 0$ ), and elliptic ( $K > 0$ ).

In case the null hypothesis of the Chi-Square ratio test is rejected, third and fourth order terms of the Taylor's expansion model can be considered to automatically proceed to the object segmentation. As reported in the literature (e.g. Cazals and Pouget, 2007), third and fourth order series can be exploited to detect ridges, crest lines and their properties. Moreover, to correctly determine discontinuity lines, some emphases on the definition of the *Monge frame* and on the computation of the Taylor's series higher order terms in this frame, are stressed. The numerical testing of the proposed procedure has been achieved with satisfactory results for real noisy data acquired with the Riegl Z390I laser scanning system and relating to the complex apse surface of the Church of Saint Anthony Abbot in San Daniele del Friuli (Italy).

## 2. LOCAL SURFACE NON PARAMETRIC ESTIMATION

Let us consider the following polynomial model of second order terms (Crosilla, Visintini and Sepic, 2008, 2009):

$$Z_j = a_0 + a_1u + a_2v + \frac{1}{2}a_3u^2 + a_4uv + \frac{1}{2}a_5v^2 + \varepsilon_j \quad (1)$$

where the coefficients and the parameters are locally related to a measured value  $Z_j$  by a Taylor's expansion of the function  $Z = \mu + \varepsilon$  in a surrounding point  $i$  of  $j$ , as:

$$a_0 = Z_{0i}; \quad a_1 = \left( \frac{\partial Z}{\partial X} \right)_{X_i}; \quad a_2 = \left( \frac{\partial Z}{\partial Y} \right)_{Y_i}$$

$$a_3 = \left( \frac{\partial^2 Z}{\partial X^2} \right)_{X_i}; \quad a_4 = \left( \frac{\partial^2 Z}{\partial X \partial Y} \right)_{X_i, Y_i}; \quad a_5 = \left( \frac{\partial^2 Z}{\partial Y^2} \right)_{Y_i}$$

$$u = (X_j - X_i); \quad v = (Y_j - Y_i)$$

with  $X_i, Y_i$  and  $X_j, Y_j$  plane coordinates of points  $i$  and  $j$ .

The parameter  $a_0$  is the estimated function value  $Z_{0i}$  at point  $i$ , while the parameters  $a_s$ , with  $s > 0$ , are the first and second

order partial derivatives along  $X, Y$  directions at the  $i$ -th point of the best approximating local surface.

Rewriting model (1) in algebraic form as:

$$z = \mathbf{X}\boldsymbol{\beta} + v \quad (2)$$

the unknown parameters are collected into the  $[6 \times 1]$  vector:

$$\boldsymbol{\beta} = [a_0 \ a_1 \ a_2 \ a_3 \ a_4 \ a_5]^T \quad (3)$$

while, considering the  $p$  neighbour points  $j$  of point  $i$ , the coefficient matrix  $\mathbf{X}$  has  $p$  rows as:

$$\mathbf{X}_j = \begin{bmatrix} 1 & u & v & \frac{1}{2}u^2 & uv & \frac{1}{2}v^2 \end{bmatrix} \quad (4)$$

In order to weight the different  $Z_j$  values for the least squares estimation of  $\boldsymbol{\beta}$ , a diagonal weight matrix  $\mathbf{W}$  is assumed by using a symmetric kernel function centred at the  $i$ -th point as:

$$w_{ij} = \left[1 - (d_{ij}/b)^3\right]^3 \text{ for } d_{ij}/b < 1$$

$$w_{ij} = 0 \text{ for } d_{ij}/b \geq 1$$

where  $d_{ij}$  is the distance between the points  $i, j$  and  $b$  is the radius (*bandwidth*) of the sphere encompassing the  $p$  closest points to  $i$ . The weighted least squares estimate of the unknown vector  $\boldsymbol{\beta}$  from  $p$  neighbour points hence results as:

$$\hat{\boldsymbol{\beta}} = (\mathbf{X}^T \mathbf{W} \mathbf{X})^{-1} \mathbf{X}^T \mathbf{W} \mathbf{z} \quad (5)$$

The residual vector  $\hat{v}$  for the  $p$  points is given as  $\hat{v} = z - \mathbf{X}\hat{\boldsymbol{\beta}}$ .

Thus, the a posteriori variance factor  $\hat{\sigma}_0^2$  at point  $i$  is given as:

$$\hat{\sigma}_0^2 = \frac{\hat{v}^T \mathbf{W} \hat{v}}{p-6} \quad (6)$$

This value has to be suitably evaluated for each point  $i$ , in order to verify by a  $\chi^2$  test if it is comparable to the measurement noise or if it is sensible also to a systematic effect, due to limitations in the Taylor's expansion order, or due to the presence of possible outliers or data slips.

### 3. TESTING THE FULFILLMENT OF THE APPLIED MODEL

For each laser point  $i$ , the estimated value of the variance factor  $\hat{\sigma}_0^2$  is crucial to verify whether the behaviour of the residuals of the encompassing bandwidth points,  $\hat{v} = z - \mathbf{X}\hat{\boldsymbol{\beta}}$ , are due to the noise of the laser measures, to possible outliers, or rather to limitations in the non parametric model. For such aim, the following Chi-Square test is applied, with null hypothesis  $H_0$ :  $\hat{\sigma}_0^2 = \sigma_{ls}^2$  and alternative hypothesis  $H_1$ :  $\hat{\sigma}_0^2 \neq \sigma_{ls}^2$ .

$$\frac{\hat{\sigma}_0^2}{\sigma_{ls}^2} (p-6) \leq \chi_{(p-6), 1-\alpha}^2 \quad (7)$$

where:

- $\sigma_{ls}^2$  is the variance of the laser scanning ( $ls$ ) instrument employed for the data acquisition;
- $\chi_{(p-6), 1-\alpha}^2$  is the Chi-Square distribution value for  $(p-6)$  degrees of freedom and  $\alpha$  probability for a first kind error.

The following analysis of the Chi-Square test results can be done, considering that if:

- $H_0$  is accepted: a good local congruence between laser measures and a second order model is statistically proved. The values derived from vector  $\hat{\boldsymbol{\beta}}$ , as the *Gaussian* and *mean* curvatures, are statistically meaningful and in such zones a curvature based classification can be carried out.
- $H_0$  is rejected; the local congruence between laser measures and the Taylor's model is not statistically fulfilled, i.e. a significant difference between the acquired laser data and the second order polynomial modeling is present. A part the reasons for this discrepancy, the derived curvature values in such zones have to be interpreted with particular care.

In general,  $\hat{\sigma}_0^2$  significantly differ from  $\sigma_{ls}^2$  along the lines of discontinuity of the scanned objects or along ridges or crest lines. This might be explainable as a not sufficient modeling of the Taylor's order terms or as an improper choice of the bandwidth radius, as will be seen in the numerical experiments.

### 4. COMPUTATION AND SIGNIFICANCE ANALYSIS OF THE CURVATURE VALUES

For the local shape analysis of laser point cloud, local *Gaussian*, *mean* and *principal* curvatures values are taken into account. Starting from the  $a_s$  terms of the estimated vector  $\hat{\boldsymbol{\beta}}$ , the following expressions for the *Gaussian*  $K$  and the *mean*  $H$  curvatures can be obtained:

$$K = \frac{a_3 a_5 - a_4^2}{(a_1^2 + 1 + a_2^2)^2} \quad (8)$$

$$H = \frac{a_3(1 + a_2^2) + a_5(1 + a_1^2) - 2a_1 a_2 a_4}{2(a_1^2 + 1 + a_2^2)^{3/2}} \quad (9)$$

The covariance matrix of these curvature values can be computed applying the variance-covariance propagation law to the same vector  $\hat{\boldsymbol{\beta}}$ . Let rewrite  $\hat{\boldsymbol{\beta}} = [\hat{z}_0 \ \hat{a}_1 \ \hat{a}_2 \ \hat{a}_3 \ \hat{a}_4 \ \hat{a}_5]^T$  in the partitioned form  $\hat{\boldsymbol{\beta}} = [\hat{z}_0 \ \hat{\mathbf{a}}]^T$  sharing the estimated function value  $\hat{z}_0$  from the sub vector  $\hat{\mathbf{a}}$  of the Taylor's expansion differential terms at point  $i$ . Let  $\boldsymbol{\Sigma}_{\beta\beta}$  be the estimated variance-covariance matrix of vector  $\hat{\boldsymbol{\beta}}$  terms; also it can be partitioned as:

$$\boldsymbol{\Sigma}_{\beta\beta} = \begin{bmatrix} \sigma_{z_0}^2 & \boldsymbol{\sigma}_{z_0 \mathbf{a}}^T \\ \boldsymbol{\sigma}_{z_0 \mathbf{a}} & \boldsymbol{\Sigma}_{\mathbf{a}\mathbf{a}} \end{bmatrix} \quad (10)$$

where  $\boldsymbol{\Sigma}_{\mathbf{a}\mathbf{a}}$  is the variance-covariance matrix of the sub vector  $\mathbf{a}$  containing the differential terms at point  $i$ . As known, the variance-covariance matrix  $\boldsymbol{\Sigma}_{\beta\beta}$  can be expressed as:

$$\boldsymbol{\Sigma}_{\beta\beta} = \hat{\sigma}_0^2 \mathbf{N}^{-1} = \hat{\sigma}_0^2 \begin{bmatrix} n_{z_0} & \mathbf{n}_{z_0 \mathbf{a}}^T \\ \mathbf{n}_{z_0 \mathbf{a}} & \mathbf{N}_{\mathbf{a}\mathbf{a}} \end{bmatrix}^{-1} = \hat{\sigma}_0^2 \mathbf{Q}_{\beta\beta} =$$

$$= \hat{\sigma}_0^2 \begin{bmatrix} q_{z_0} & \mathbf{q}_{z_0 \mathbf{a}}^T \\ \mathbf{q}_{z_0 \mathbf{a}} & \mathbf{Q}_{\mathbf{a}\mathbf{a}} \end{bmatrix} \quad (11)$$

where  $\mathbf{Q}_{\beta\beta}$  is the covariance matrix of vector  $\hat{\boldsymbol{\beta}}$ , while  $\hat{\sigma}_0^2$  is given by the relationship (6).

The estimated *Gaussian* and *mean* curvature values are not independent, as can be seen observing equations (8) and (9). In order to apply a significance test taking in account also the correlation between the curvature values  $K$  and  $H$ , the following

[2 x 1] vector is introduced:

$$\boldsymbol{\omega} = [K \quad H]^T \quad (12)$$

Applying the variance-covariance propagation law, the covariance matrix of vector  $\boldsymbol{\omega}$  can be obtained as:

$$\boldsymbol{Q}_{\boldsymbol{\omega}\boldsymbol{\omega}} = \boldsymbol{F}_{\boldsymbol{\omega}\boldsymbol{\omega}} \boldsymbol{Q}_{aa} \boldsymbol{F}_{\boldsymbol{\omega}\boldsymbol{\omega}}^T \quad (13)$$

where:

$$\boldsymbol{F}_{\boldsymbol{\omega}\boldsymbol{\omega}} = \begin{bmatrix} \frac{\partial K}{\partial a_1} & \frac{\partial K}{\partial a_2} & \frac{\partial K}{\partial a_3} & \frac{\partial K}{\partial a_4} & \frac{\partial K}{\partial a_5} \\ \frac{\partial H}{\partial a_1} & \frac{\partial H}{\partial a_2} & \frac{\partial H}{\partial a_3} & \frac{\partial H}{\partial a_4} & \frac{\partial H}{\partial a_5} \\ \frac{\partial a_1}{\partial a_1} & \frac{\partial a_2}{\partial a_2} & \frac{\partial a_3}{\partial a_3} & \frac{\partial a_4}{\partial a_4} & \frac{\partial a_5}{\partial a_5} \end{bmatrix}$$

In conclusion, for the points where the null hypothesis of the  $\chi^2$  test (7) is fulfilled, to verify whether the *Gaussian* and *mean* curvature vector  $\boldsymbol{\omega}$  is significantly different from zero, the alternative hypothesis of the following *F* ratio test must be satisfied (Pelzer, 1971), with null hypothesis  $H_0: E(\boldsymbol{\omega})=0$  and alternative hypothesis  $H_1: E(\boldsymbol{\omega}) \neq 0$ :

$$\frac{\boldsymbol{\omega}^T \boldsymbol{Q}_{\boldsymbol{\omega}\boldsymbol{\omega}}^{-1} \boldsymbol{\omega}}{r \hat{\sigma}_0^2} > F_{1-\alpha, r, \infty} \quad (14)$$

where:

- $r = \text{rank}(\boldsymbol{Q}_{\boldsymbol{\omega}\boldsymbol{\omega}}) = 2$ ,
- $F_{1-\alpha, r, \infty}$  Fisher distribution value for  $r$  and  $\infty$  degrees of freedom and  $\alpha$  probability for a first kind error.

## 5. SIGNIFICANCE ANALYSIS OF THE CURVATURE BASED CLASSIFICATION

If  $E(\boldsymbol{\omega}) \neq 0$ , it is worthwhile to independently test the values of  $K$  and  $H$ , in order to check if both, or just only one of them, are significantly different from zero. The null hypothesis is separately rejected for  $K$  and  $H$ , i.e.  $E(K) \neq 0$ ,  $E(H) \neq 0$ , if:

$$\frac{K^2}{\hat{\sigma}_0^2 q_{kk}} > F_{1-\alpha/2, 1, \infty} \quad (15.1)$$

$$\frac{H^2}{\hat{\sigma}_0^2 q_{hh}} > F_{1-\alpha/2, 1, \infty} \quad (15.2)$$

where:

- $q_{kk}$  and  $q_{hh}$  are the diagonal terms of matrix  $\boldsymbol{Q}_{\boldsymbol{\omega}\boldsymbol{\omega}}$ ,
- $F_{1-\alpha/2, 1, \infty}$  Fisher distribution value for 1 and  $\infty$  degrees of freedom and  $\alpha/2$  probability for each of the two tests in order to satisfy a global first kind error value equal to  $\alpha$  (Bonferroni correction).

By simultaneously analyzing the sign and the values of  $K$  and  $H$ , a statistically proven classification of the whole point cloud is finally made possible. In fact, as known, each surface can be classified as one of the following types (see Table 1): hyperbolic (if  $K < 0$ ), parabolic ( $K = 0$  but  $H \neq 0$ ), planar ( $K = H = 0$ ), and elliptic ( $K > 0$ ).

When the null hypothesis  $H_0: K = 0$  is only satisfied, if  $H > 0$  the single curvature surface can be classified as a concave parabolic valley, while if  $H < 0$  as a convex parabolic ridge. Finally whether both null hypotheses are rejected, the surface is classifiable as a concave pit (if  $K > 0$  and  $H > 0$ ), as a convex peak ( $K > 0, H < 0$ ), as a saddle valley ( $K < 0, H > 0$ ), or as a saddle ridge ( $K < 0, H < 0$ ).

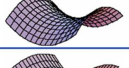
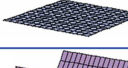
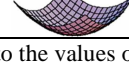
	$K < 0$ : hyperbolic	$K = 0$ : parabolic/planar	$K > 0$ : elliptic
$H < 0$			
$H = 0$			not possible
$H > 0$			

Table 1: Classification of surfaces according to the values of *Gaussian*  $K$  and *mean*  $H$  curvatures (from Haala et al., 2004).

As reported in Crosilla, Visintini and Sepic (2008, 2009), the subsequent automatic modeling of each recognized unit is performed by estimating the corresponding surface analytical function, starting from raw clusters detected by a region growing method. Furthermore, the automatic segmentation of geometrical units can be indirectly obtained by means of 3D spatial intersections among the estimated surfaces.

## 6. ESTIMATING HIGHER ORDER TERMS OF THE TAYLOR'S EXPANSION

As reported in the literature (e.g. Cazals and Pouget, 2003), ridges are curves along which one of the *principal curvatures* has an extremum along its curvature values. For this reason, their location requires estimating differential quantities up to the third order, and actually up to the fourth order to decide whether the extremum is a maximum or a minimum. Furthermore, ridges can furnish information for the laser point clouds segmentation, registration and matching procedures. As ridges are detected analyzing the principal curvature values, it is necessary to adopt for each point, where the Taylor's expansion is applied, a local reference system able to directly furnish principal curvature values and their directional derivatives. This coordinate system is the so-called "*Monge frame*", where the terms  $a_0, a_1, a_2, a_4$  are equal to zero. The Taylor's expansion up to the fourth order terms assumes the following expression:

$$Z_j = \frac{1}{2}(a_3 u^2 + a_5 v^2) + \frac{1}{6}(b_0 u^3 + 3b_1 u^2 v + 3b_2 u v^2 + b_3 v^3) + \frac{1}{24}(c_0 u^4 + 4c_1 u^3 v + 6c_2 u^2 v^2 + 4c_3 u v^3 + c_4 v^4) + \varepsilon_j \quad (16)$$

where:

- $a_3, a_5$  correspond, in the Monge frame, to the *principal curvatures*;
- $b_0, b_3$  are the directional derivatives of  $a_3, a_5$  along their respective curvature lines;
- $b_1, b_2$  are the directional derivatives of  $a_3, a_5$  along the other curvature lines.

Points having an extremum value for  $b_0$  or  $b_3$  automatically identify ridges. Specific algorithms to perform the curvature estimation of the differential terms in the *Monge frame* and to automatically extract ridges have been recently proposed in the literature (Cazals and Pouget, 2007). The analytical process is complex since it requires the following four steps algorithm.

### 6.1 Principal Component Analysis

First step performs a Principal Component Analysis (PCA) for each sampled point, relating to its surrounding ones. This analysis allows to determine three orthogonal eigenvectors and the associated eigenvalues. If the surface is well sampled, PCA provides one small and two large eigenvalues. The eigenvector associated to the small one approximates the normal vector.

## 6.2 Roto-translation of the coordinate frame

At the second step, a change of coordinates is executed, to move the original values into a new frame ( $S$ ), having as origin the point at which the estimation is performed. A polynomial fitting as (1) extended to fourth order terms, is then carried out.

## 6.3 Computation of the Monge basis

Third step allows to determine the Monge basis by computation of the normal direction to the estimated surface, by a symmetrization and diagonalization process of the so called "Weingarten matrix"  $A$  (e.g. Do Carmo, 1976) transformed in the orthonormal basis of the tangent space.

Normal direction  $\mathbf{n}$  is defined by the vector:

$$\mathbf{n} = \frac{1}{\sqrt{a_1^2 + 1 + a_2^2}} \begin{bmatrix} -a_1 & -a_2 & 1 \end{bmatrix}^T \quad (17)$$

The symmetrization is carried out, first by computing an orthonormal basis of the tangent plane applying the Gram-Schmidt algorithm to the tangent plane basis:

$$\{\mathbf{u}, \mathbf{v}\} = \left\{ \begin{bmatrix} 1 & 0 & a_1 \end{bmatrix}^T, \begin{bmatrix} 0 & 1 & a_2 \end{bmatrix}^T \right\} \quad (18)$$

in which the Weingarten matrix  $A$  is originally computed. After that, calling  $\mathbf{G}$  the upper sub matrix  $[2 \times 2]$  of the  $[3 \times 2]$  orthonormal basis of the tangent plane, the symmetric Weingarten matrix  $A_{sym}$  is computed from (Cazals and Pouget, 2007):

$$A_{sym} = \mathbf{G}^{-1} \mathbf{A} \mathbf{G} \quad (19)$$

The *principal* curvatures are obtained from a diagonalization of matrix  $A_{sym}$  since corresponding to its eigenvalues, while the principal directions are given by the eigenvectors of  $A_{sym}$ .

## 6.4 Principal curvatures directional derivatives computation

Finally directional derivatives  $b_0, b_3$  of the *principal* curvatures are computed by differentiating the implicit equation of the fitted polynomial surface in the Monge basis. This last one is obtained by applying a parameter transformation to the equation of the fitted polynomial defined in the  $S$  frame used to compute the Weingarten matrix  $A$ .

From the implicit function theorem (e.g. Do Carmo, 1976), the surface  $f(X, Y, Z) = 0$  can be locally written as the graph of the height function  $Z = g(X, Y)$ . The directional derivatives  $b_0, b_3$  in the Monge frame are finally obtained by applying the chain rule while differentiating the equation  $f(X, Y, g(X, Y)) = 0$ .

## 7. NUMERICAL EXPERIMENTS

The automatic analytical model proposed has been implemented in a C language program and so some numerical experiments have been carried out and are now presented.

Dataset regards real laser scanning points acquired with the Riegl Z390I system into the Church of Saint Anthony Abbot in San Daniele del Friuli (Italy). The detailed description of the church, of the laser scanning and photogrammetric surveying, and of the photorealistic VRML/X3D modeling is reported in Visintini, Siotto and Menean (2009), in this proceedings volume. The rectangular presbytery and the pentagonal apse are upper closed by a composed surface and are decorated with very important Renaissance frescoes painted by Martino da Udine (1467-1547): in particular, the apse ceiling is shaped by a rib vault with eight sails (see Figure 2 at left).

The laser point cloud of about 70.000 points submitted to the

numerical experiments regards the final part of the apse, with three portions of vertical walls, five parts of vault sails (cloves), and six ribs, two entire and four clipped, converging into the circular medallion in the dome apex (see Figure 2 at right).

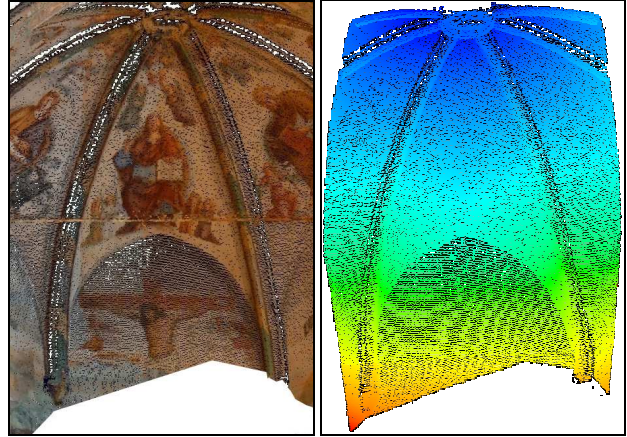


Figure 2: Laser points of the apse of the Church of St. Anthony Ab. in S.Daniele (l) coloured by RGB (at left) and by Z (at right).

The points were acquired from the centre of the apse with the principal axes of the laser scanning system turned of  $90^\circ$ , i.e. horizontal, and with an angular step of  $0,120^\circ$  so obtaining a very high density on the apse surface, meanly of about 5.500 points per square meter. Such points are coloured in Figure 2 at right according to their Z value, from blue ( $-6,67$  m) to red ( $-3,24$  m): it means that, to fruitfully apply Taylor's expansion (1), Z vertical axis has been simply flipped from upward (zenith) to downward (nadir), without any other rotation.

## 7.1 Computation and statistical analysis of curvature values

Using a bandwidth sphere radius  $b = 10$  cm, so encompassing meanly a number  $p$  of about 170 points, the local unknown vectors  $\hat{\beta}$  have been estimated by (5), while the local variance factors  $\hat{\sigma}_0^2$  by (6); these lasts are shown in Figure 3 at left.

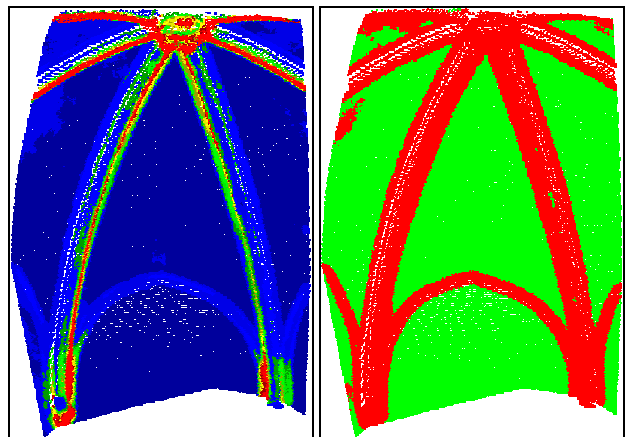


Figure 3: Points coloured by  $\hat{\sigma}_0^2$  values (at left), from blue to red, and by  $\chi^2$  test results (at right), green = H0, red = H1.

As can be seen, most part of points are blue coloured (dark blue corresponds to zero), for instance about 52.000 points (75% of dataset) have a  $\hat{\sigma}_0$  less than  $\pm 7$  mm, numerically evidencing a general correctness of the adopted second order non parametric model. Points coloured in red, having maximum values of  $\hat{\sigma}_0^2$ , are about 3.000 (4% of dataset) with  $\hat{\sigma}_0$  ranging from  $\pm 23$  mm to  $\pm 56$  mm: such points are located in the ribs where these,

occluding the scanning surveying, cause data slips in Z values. Nevertheless, to statistically verify the model fulfilment, the Chi-Square test (7) has been carried out considering a  $\sigma_{ls}^2$  value equal to  $0,16 \text{ cm}^2$  (i.e.  $\sigma_{ls} = \pm 4 \text{ mm}$ ). The results are shown in Figure 3 at right: the green points, representing the local acceptance of the null hypothesis, are 64% of the dataset and are located on the regular surfaces, i.e. in the frescoes scenes. The red points, where the test fails, put in evidence that  $\hat{\sigma}_0^2$  is locally significantly higher than  $\sigma_{ls}^2$  and this happens along the ribs and their surroundings.

A thought arises from the obtained results for variance factor and Chi-Square test: in the buffer zones around the intersections between two regular surfaces, e.g. in the arcs, the width of unsatisfactory  $\hat{\sigma}_0^2$  and rejection  $\chi^2$  areas corresponds about to the bandwidth radius  $b$ . These refusal areas might be reduced by choosing a smaller value for  $b$ , as will be later shown.

Going on with a 10 cm bandwidth radius, Figure 4 shows the estimated Gaussian curvature values [ $\text{m}^{-2}$ ], while Figure 5 those of the mean curvature [ $\text{m}^{-1}$ ]. For a qualitative evaluation of these results, the shape of the apse sails has been reasonably supposed as constituted by two double curvature concave surfaces, starting from an acute arc onto the planar wall, and ramping up to the apex node. In truth, some constructive irregularities can be visually perceived *in situ* in the vertical walls, while it is quite impossible to recognize deformations in the higher twofold curved and frescoed sails.

The values of Gaussian K curvature in Figure 4 at left, a part in the edges zones, are mainly coloured in green, corresponding to the interval  $-0,1 \div 0,0$ , and in brown, relating to the interval  $0,0 \div 0,1$ , as can be better seen in Figure 4 at right, where only such little values of K are depicted. These last K values stand for principal curvature radii of a size from 3,16 m to infinite, i.e. low curved or planar surfaces. Nevertheless, their variability from negative to positive sign among near points, confirms the requirement to carry out a statistical analysis of the K values.

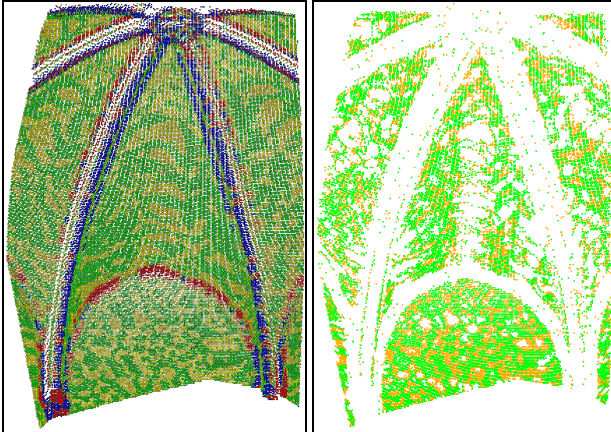


Figure 4: Points coloured by K values, from blue to red (at left) and only for  $K \in -0,1 \div 0,0$  (green) and  $0,0 \div 0,1$  (brown) (at right).

For a better qualitative evaluation of the mean H results, coloured from blue to red in Figure 5 at left, only some values around zero are reported in Figure 5 at right: in particular, the interval  $-2,5 \div -0,2$  in red,  $-0,2 \div 0,2$  in green and  $0,2 \div 2,5$  in yellow. For red and yellow points the principal curvature radii have a size from 0,4 to 5,0 m, while is higher for the green ones, i.e. very low curvatures. A chromatic exam puts in evidence that mainly  $H \in -0,2 \div 0,2$  (green) for the planar areas, and this is correct; for the vault sails, where  $H > 0$  values are expected, not only higher positive (yellow) values but also higher negative

(red) ones result, i.e. the surface is concave and convex. Surprisingly, after a careful visual evaluation of the TIN model of such points and also by transversal sections, such estimated convex shapes have been confirmed for each vault sail!

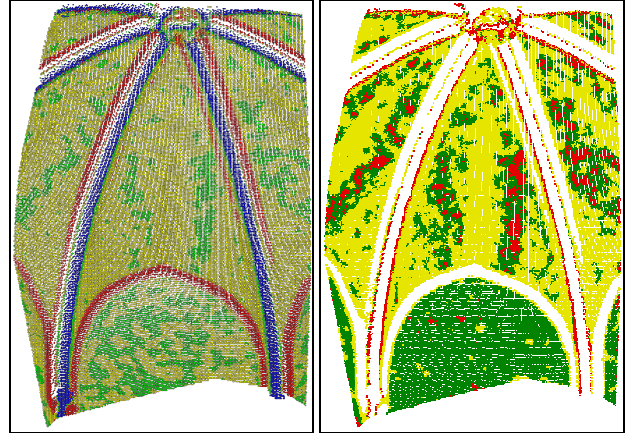


Figure 5: Points coloured by H values (at left) and only for  $H \in -2,5 \div -0,2$  (red),  $-0,2 \div 0,2$  (green) and  $0,2 \div 2,5$  (yellow) (at right).

Coming back to Figure 5 at left, in the buffer areas around the intersections among different surfaces, although  $\chi^2$  test evidences that the second order expansion model should be extended with higher order terms, the underestimated H values are so large to anyway suggest the presence of convex edges in blue (where  $H < -4,5$ ) and concave edges in red (where  $H > 5,0$ ).

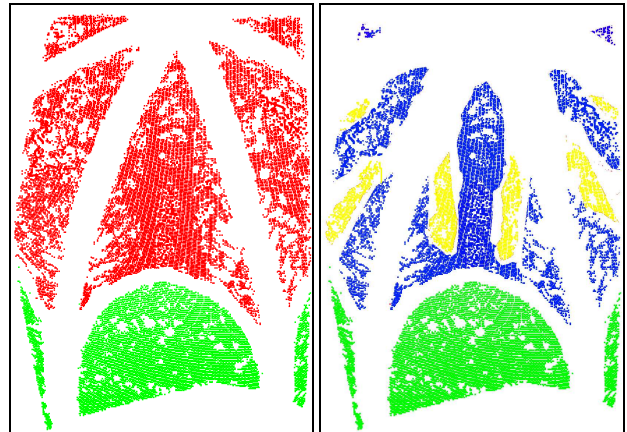


Figure 6: Points coloured by F ratio test results (at left), green = H0, red = H1, and by classified surface types (at right).

The results of the F ratio test (14), onto points satisfying the Chi-Square test, are depicted in Figure 6 at left: adjacent points with the same answer, but creating areas smaller than  $b^2$ , are prudentially omitted. The percent of green points where H0 is accepted is 39%, and correctly corresponds to the planar areas, while red points, meaning curved surfaces, ensue as 71%.

Last but not least, Figure 6 at right shows the obtained point classification: planes are in green, concave pits in blue, and saddle ridges in yellow. For caution, classified points forming too small clusters (area  $< b^2$ ) remain unclassified (white).

## 7.2 Optimization of the classification process

An automatic classification process should be followed from the automatic modeling of the classified points, at least from the mathematical point of view. In any case, the automatic classification of the higher part of a point cloud is an essential task. To reach such a goal with the proposed method, given a certain dataset, the size of the bandwidth radius  $b$  is

determinant. Figure 7 depicts the results obtained with a new numerical experiment carried out with  $b$  reduced to 5 cm.

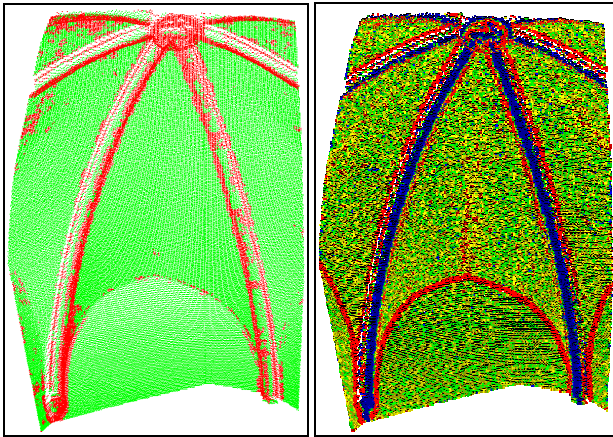


Figure 7: Points coloured by  $\chi^2$  test results (at left) and  $H$  values (at right), from blue to red, with a bandwidth  $b = 5$  cm.

As can be seen at left, with respect to Figure 3 at right, the percent of green points where the  $\chi^2$  test  $H_0$  hypothesis holds, grows to 83%: also for most part of the arc points, the second order model is statistically sufficient to locally describe the surface. In Figure 7 at right, the high values of  $H$ , red colored if  $H > 8,0$ , correctly indicate the presence of the arc concave edges. Figure 8 concerns the most complicated part of the dataset, namely the medallion where the ribs are connected, submitted to a third experiment with a bandwidth further on limited to 3 cm.

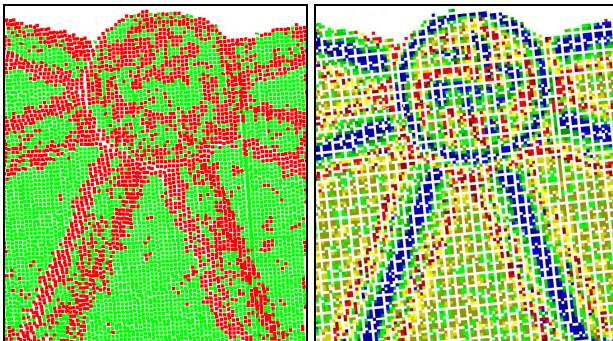


Figure 8: Enlargement of apex points coloured by  $\chi^2$  test results (at left) and  $H$  values (at right), with  $b = 3$  cm.

The  $H_0$  prevalent result of the  $\chi^2$  test (at left) for the central part of the ribs affirms as significant the obtained  $H$  values (at right). Blue colour corresponds to  $H < -15$ , namely a convex surface with a principal curvature radius size less than 6,6 cm: this fully agrees with some measures in the point cloud. Moreover, the torus border of the medallion is yet blue coloured: for some points  $H < -20$ , i.e. a curvature radius size less than 5 cm. Concluding, by using centimetric values of  $b$ , surfaces with centimetric curvature radius can be modeled. Off course, the reduction of the bandwidth radius has a drawback: it leads to a low redundancy ( $p - 6$ ) in the estimation of  $\beta$  and all the curvature values derived from, and this is quite thoughtless in processing real noisy laser datasets.

A strategy to find the optimal bandwidth radius could be to start with a rather large value  $b$  able to classify at least 50% of points, and to reduce it until the Chi-Square test fails, rejecting points belonging to surfaces already classified with a larger  $b$ . Summarizing, a large part of real laser points of St. Anthony Church apse have been directly classified by means of the

proposed method: for unclassified points, i.e. where non parametric model results are not reliable, the automatic classification can be done by a robust parametric modeling, as described in Crosilla, Visintini and Sepic (2008, 2009).

## 8. CONCLUSIONS

The paper proposes a procedure based on a statistical analysis able to automatically detect reliable *Gaussian* and *mean* curvature values for laser point clouds, computed by applying a local surface non parametric Taylor's expansion.

First, the fulfilment of the analytical model applied is verified by a Chi-Square test comparison of the a priori and a posteriori variance factors. A second test considers the variance-covariance propagation law applied to the estimated Taylor's terms, in order to compute the covariance matrix of the *Gaussian* and *mean* curvature values. If the null hypothesis of the applied  $F$  test is rejected, at least one curvature value is significantly different from zero and the sign analysis allows to classify the geometrical shape of each object surface unit.

A fascinating procedure to automatically detect discontinuity lines is then presented. By the analysis of higher order terms of a Taylor's expansion expressed in the Monge frame, it is possible to detect points characterized by the highest values of *principal* curvature directional derivatives.

The carried out numerical experiments on real laser data of a complex surface show the capabilities of the proposed method.

## REFERENCES

- Cazals, F., Pouget, M., 2003. Estimating differential quantities using polynomial fitting of osculating jets. In: *Proceedings of the 1st Symposium on Geometry Processing*, pp. 177-187.
- Cazals, F., Pouget, M., 2007. *Jet\_fitting\_3*: A generic C++ package for estimating the differential properties on sampled surfaces via polynomial fitting. Rapport de recherche 6093, INRIA, France.
- Crosilla, F., Visintini, D., Sepic, F., 2008. A statistically proven automatic curvature based classification procedure of laser points. In: *The Int. Arch. of Photogrammetry, Remote Sensing and Spatial Information Sciences*, Beijing, China, Vol. XXXVII, Part B5, pp. 469-475 (on CD).
- Crosilla, F., Visintini, D., Sepic, F., 2009. Reliable automatic classification and segmentation of laser point clouds by statistical analysis of surface curvature values. *Applied Geomatics*, International Journal of the Italian Society of Photogrammetry and Topography, Springer, (in press).
- Do Carmo, M.P., 1976. *Differential geometry of curves and surfaces*. Prentice-Hill International, London.
- Haala, N., Reulke, R., Thies, M., Aschoff, T., 2004. Combination of terrestrial laser scanning with high resolution panoramic images for investigations in forest applications and tree species recognition. In: *The Int. Arch. of Photogrammetry, Remote Sensing and Spatial Information Sciences*, Dresden, Germany, Vol. XXXIV, Part 5/W16.
- Pelzer, H., 1971. *Zur analyse geodätischer deformationsmessungen*. DGK, Reihe C, 164, München.
- Visintini, D., Siotto, E., Menean, E., 2009. 3D modeling of the St. Anthony Abbot Church in S. Daniele del Friuli (I): from laser scanning and photogrammetry to VRML/X3D model. In: *The Int. Arch. of Photogrammetry, Remote Sensing and Spatial Information Sciences*, Trento, Italy, Vol. XXXVIII, Part 5/W1 (this volume).